journal

J. Am. Ceram. Soc., 1–8 (2013)
DOI: 10.1111/jace.12488

Comparison of Two-Phase Thermal Conductivity Models with Experiments on Dilute Ceramic Composites

Jesse P. Angle,[‡] Zhaojie Wang,[§,¶] Chris Dames,[¶] and Martha L. Mecartney[‡,†]

[‡]Department of Chemical Engineering and Materials Science, University of California, Irvine, California 92697

[§]Department of Mechanical Engineering, University of California, Riverside, California 92521

[¶]Department of Mechanical Engineering, University of California, Berkeley, California 94720

Thermal shock resistance of cubic 8 mol% yttria-stabilized zirconia (YSZ) can be increased by the addition of dilute second phases. This study addresses how these dilute second phases affect the thermal conductivity for two-phase ceramic composites of 8 mol% YSZ with 10–20 vol% alumina (Al_2O_3) or 10–20 vol% mullite ($3Al_2O_3{\cdot}2SiO_2$). Thermal conductivity measurements from 310 K (37°C) to 475 K (202°C) were made using the 3ω method and compared with results from 3D analytical models and a 2D computational microstructure-based model (Object-Oriented Finite Element Analysis, OOF2). The linear Rule of Mixtures was the least accurate and significantly overestimated the measured thermal conductivity at low temperatures, with errors in some cases exceeding 100%. Calculations using the Bruggeman and OOF2 models were both much better, and the deviation of less than ±2.5% across all compositions and temperatures is within the range of experimental and modeling uncertainty. The Maxwell Garnett equation was a close third in accuracy (±8%). A sensitivity analysis for each model quantifies how small perturbations in the thermal conductivity of the dispersed second phase influence the effective thermal conductivity of the composite, and reveals that the linear Rule of Mixtures model is physically unrealistic and oversensitive to the thermal conductivity of the dispersed phase.

I. Introduction

The effect of second phases on sintering, mechanical properties, and ionic conductivity of cubic 8 mol% yttria-stabilized zirconia (8 mol% YSZ) has been of strong interest[1–4] as commercial applications for cubic 8 mol% YSZ include solid oxide electrolytes for oxygen sensors and fuel cells.[5–8] Yet, although thermal shock is one of the most common operational failure modes for 8 mol% YSZ oxygen sensors, relatively little work has been conducted on how second phases in YSZ affect thermal shock. Thermal shock and failure occur during rapid cooling for temperature differences as small as 100 K for single phase 6 mol% cubic YSZ[9] and 150 K for single phase 8 mol% cubic YSZ.[10]

Dilute second phase additions of alumina in 8 mol% YSZ can increase the thermal shock resistance.[10] Dilute solutions are those in which the second phase is below the percolation limit. One effect of adding a second phase with a higher thermal conductivity, such as alumina in YSZ,[11] is an increase in the effective thermal conductivity, with faster heat transfer from the interior to the exterior during quenching. Faster heat transfer reduces thermal gradients that cause residual stress due to thermal expansion. These thermal stresses are primarily responsible for crack propagation from preexisting flaws during thermal shock. To understand how second phases affect heat transport in 8 mol% YSZ in the temperature range where thermal shock occurs, an analysis of the thermal conductivity and its dependence on the microstructure, amount of second phases, and distribution of the second phase should be conducted, and is the focus of this study.

Experimental characterization of the thermal conductivity for ceramics and ceramic composites is usually performed using the laser flash method over a range of temperatures, typically 373–1273 K (100°C–1000°C).[12] At temperatures below approximately 473 K (200°C), alternative techniques such as the 3ω method can also be employed.[13–15] As YSZ has low electrical and thermal conductivity, it is a good candidate for the 3ω method, which requires only small temperature fluctuations for sensitive measurements.

Microstructure-based finite element modeling can be applied to approximate the thermal conductivity of composites and is especially useful because of its capability to account for size, shape, and distribution of second phase particles. Object-oriented finite element analysis version 2 (OOF2),[16,17] open access software developed at the National Institute of Standards and Technology (NIST), can be used effectively for this purpose. OOF2 uses two-dimensional scanning electron microscopy (SEM) microstructures as the foundation for calculations, and has been applied to successfully characterize the thermal behavior with respect to porosity in t' 4 mol% YSZ thermal barrier coatings[18] and Cu–SiC composites,[19] the latter with a honeycomb structure that allows two-dimensional modeling to be an appropriate approximation of three dimensions.

This study evaluates four theoretical methods (OOF2 simulations, Maxwell Garnett, Bruggeman, and linear Rule of Mixtures approximation) used to predict the effective thermal conductivity of composite materials. The analytical models, Maxwell Garnett, Bruggeman, and linear Rule of Mixtures only require knowledge of the three-dimensional volume fraction of each phase and the respective thermal conductivities, but do not take into consideration microstructural details. In contrast, although the OOF2 simulations are fundamentally two dimensional, they benefit from using real microstructural geometries of each phase when determining the effective thermal conductivity.

The linear Rule of Mixtures is simple, but most appropriately used when each phase is contiguous and aligned parallel to the direction of heat flow.[20] It is sometimes used for two-phase systems, randomly dispersed with respect to the heat flow, due to mathematical convenience for approximating the effective thermal conductivity (k_{eff}) based on the volume fraction of each phase. In the linear Rule of Mixtures [Eq. (1)], k_1 is the thermal conductivity of Phase 1, k_2 is the thermal

D. Smith—contributing editor

Manuscript No. 32910. Received March 19, 2013; approved June 5, 2013.
[†]Author to whom correspondence should be addressed. e-mail: martham@uci.edu

conductivity of Phase 2, and V_1 and V_2 are the respective volume fractions of the two-phases.

$$k_{\text{eff}} = k_1 V_1 + k_2 V_2 \tag{1}$$

The inverse Rule of Mixtures is appropriate when each phase is contiguous and aligned perpendicular to the direction of heat flow.[20]

$$\frac{1}{k_{\text{eff}}} = \frac{V_1}{k_1} + \frac{V_2}{k_2} \tag{2}$$

When the second phase is a low volume fraction and randomly dispersed, more appropriate equations are available for calculating effective material properties of composites, including the Maxwell Garnett and Bruggeman models.[21–23] Maxwell Garnett assumes that the dispersed phase can be represented as spheres far enough apart to have negligible thermal interactions between particles.[24] Bruggeman uses the assumption that both the components are randomly dispersed with no assumed shape, and is most accurate when one phase is below the percolation limit.[25] Both these models have been applied to determine the effective thermal conductivity in two-phase ceramic composites.[26–33] (There are more complex expressions that can be employed when the dispersed phase has a specific geometric shape such as platelets, cylinders, etc., and when intergranular phases or delamination provides high interfacial resistance.[34]) In both models, k_1 and V_1 are the thermal conductivity and volume fraction of the continuous phase (8 mol% YSZ in this case), respectively, and k_2 and V_2 are the thermal conductivity and volume fraction of the dispersed phase, respectively. The two-component Maxwell Garnett model used to calculate the effective thermal conductivity of a two-phase composite is given by Eq. (3):

$$k_{\text{eff}} = k_1 \left(\frac{k_2(1 + 2V_2) - k_1(2V_2 - 2)}{k_1(2 + V_2) + k_2(1 - V_2)} \right) \tag{3}$$

The two-component, three-dimensional Bruggeman model used to calculate effective thermal conductivity is given by Eq. (4):

$$V_1 \left(\frac{k_1 - k_{\text{eff}}}{k_1 + 2k_{\text{eff}}} \right) + V_2 \left(\frac{k_2 - k_{\text{eff}}}{k_2 + 2k_{\text{eff}}} \right) = 0 \tag{4}$$

In this study, the thermal conductivity of 8 mol% YSZ with alumina (Al_2O_3) or mullite ($3Al_2O_3{\cdot}2SiO_2$) second phase additions is measured experimentally using the 3ω method for the temperature range for thermal shock of 8 mol% YSZ. The computational finite element approach of OOF2 and the three equation-based analytical models are used to approximate the effective thermal conductivity of two-phase ceramic composites and compared with the experimental 3ω measurements. A sensitivity analysis is performed on all four theoretical models to determine the effects of small perturbations in the thermal conductivity of the second phase on the effective thermal conductivity of the composites.

II. Experimental Procedures

(1) Sample Preparation and Characterization

Ceramic powders of 8 mol% YSZ powder (Tosoh Co. Ltd., Tokyo, Japan, crystallite size of 30 nm), high-purity α-alumina powder (Baikowski Inter. Corp., Charlotte, NC, crystallite size of 40 nm), or high-purity mullite powder (KCM Corporation, Nagoya, Japan, crystallite size of 40 nm) were attritor-milled then formed into cylinders by cold isostatic pressing. Five compositions were made: (1) 8 mol% YSZ, (2) 8 mol% YSZ + 10 vol% alumina, (3) 8 mol% YSZ + 20 vol % alumina, (4) 8 mol% YSZ + 10 vol% mullite, and (5) 8 mol% YSZ + 20 vol% mullite. All were sintered at 1823 K (1550°C) for 2 h. Density was measured by the Archimedes method.

X-ray diffraction (XRD; Rigaku SmartLab X-ray Diffractometer, Tokyo, Japan) used Cu-k_α radiation (wavelength 0.15406 nm) and scans from 20° to 90° in 0.05° steps. SEM was performed using a Philips/FEI XL 30 FEG (FEI, Hillsboro, OR). A thin film of iridium was deposited on the surface (South Bay Technology IBS/e Ion Beam Sputter Deposition System, San Clemente, CA) to prevent electrical charging during SEM analysis. Grain sizes were determined by ImageJ (National Institute of Health) with values for grain diameters in two dimensions multiplied by 1.74, the mathematical relationship between a regular polyhedron and equiaxed grain diameter, to obtain a "true" three-dimensional grain size.[35]

(2) 3ω Method

Each sample was polished to a finish of 0.06 μm. A gold heater line was patterned directly onto polished surfaces by photolithography and a liftoff method with typical heater dimensions 10 μm width, 250 nm thickness, and 0.5 mm length between the inner voltage probes (Fig. 1). A 10 nm layer of chromium was used to improve adhesion between the gold and sample.

In the standard 3ω method, the oscillating temperature field varies over a length scale known as the "thermal wavelength", defined as $\lambda = \sqrt{(D/2\omega)}$, where D is the thermal diffusivity and ω is the angular frequency of the heating current.[14] The approximate range of λ in this study is estimated as 8.7 μm < λ < 47 μm, based on the range of measurement frequencies (890 Hz > ω/2π > 30 Hz) and the diffusivity of conventional YSZ ($D \approx 8.4 \times 10^{-7}$ m^2/s).[36] Since these λ values are much larger than the estimated phonon mean free paths in these materials (well below 100 nm), the continuum treatment of the standard 3ω method is justified.[37] Furthermore, the large heater length ensures that the measurement is an average over numerous grains.

To ensure the stability of the heater line's electrical resistance, the samples were annealed at 500 K (227°C) after microfabrication and before measurements. Then 3ω data were collected from 310 K (37°C) to 475 K (202°C), waiting 30 min between every temperature point to ensure thermal stability. During the experiment, the 3ω method also causes a small steady-state temperature increase in the heater line above the bulk sample temperature, with a typical value $T_{\text{Heater}} \approx T_{\text{Bulk Sample}} + 5$ K. To reflect this, data are plotted at $T_{\text{avg}} = (T_{\text{Heater}} + T_{\text{Bulk Sample}})/2$ and error bars reflect this difference between T_{Heater} and T_{avg} as well as the inherent temperature uncertainty of typically 0.5%.

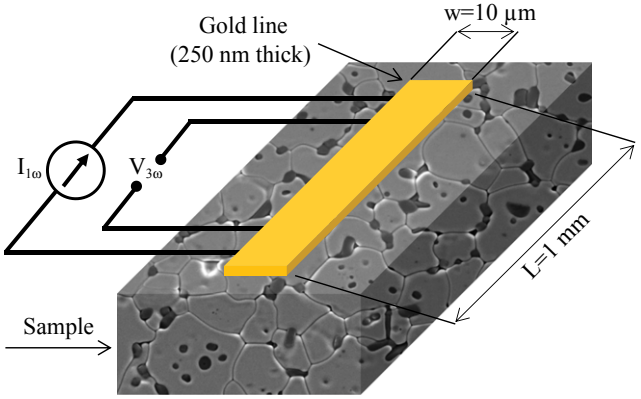

Fig. 1. Schematic of a typical 3ω measurement setup. Not to scale. Typical sample thickness is 3 mm.

(3) Object-Oriented Finite Element Analysis Version 2 Simulations

A thermal gradient model was produced using OOF2 for each composition. Two-dimensional SEM images are converted to two-color images to create finite element meshes adapted to the microstructure of the material. Each phase is represented by a single color value and assigned input values for thermal conductivity as a function of temperature from experimental results on single-phase materials.[38–40]

A thermal gradient is simulated in the vertical direction of the image by assigning the top boundary a fixed temperature value and the bottom boundary a value 10 K higher, keeping the other two sides adiabatic. The heat equation is solved by the conjugate gradient method, resulting in an x and y heat flux component assigned to each node of the mesh. OOF2 removes the third dimension by setting the out-of-plane (z) heat flux components to zero, analogous to plane stress analysis used in fracture mechanics. The resulting 2D heat flux is integrated across the top to determine the effective thermal conductivity:

$$k_{\text{eff}} = \frac{L_y Q}{L_x (T_{\text{bottom}} - T_{\text{top}})} \tag{5}$$

where k_{eff} is the effective thermal conductivity of the composite, Q (watts per meter of thickness in z) is the OOF2 heat flux integrated across the top boundary, L_y and L_x are the image dimensions, and T_{bottom} and T_{top} are the temperature values assigned to the bottom and top boundaries. By simulating a thermal gradient across an image, k_{eff} is calculated at various temperatures from 298 to 473 K (25°C–200°C). Three representative SEM micrographs were used for each composition to calculate the average effective thermal conductivity. Typical variability between each simulation for the same composition was less than 1%.

(4) Dimensionless Sensitivity Analysis

The dimensionless sensitivity parameter, S_{k_i}, is the fractional change in k_{eff} when the thermal conductivity of a specific phase (i = continuous or dispersed) is perturbed while the other held constant. For example, if a 1% change in k_2 leads to a corresponding 1% change in k_{eff}, then the dimensionless sensitivity parameter is $S_{k_2} = 1$, meaning k_{eff} is fully sensitive to k_2. Likewise, if $S_{k_2} = 0.3$, then a 1% change in k_2 would cause a 0.3% change in k_{eff}. Mathematically, the sensitivity of k_{eff} to changes in the thermal conductivity of the dispersed phase (k_2) is as follows:

$$S_{k_2} = \frac{k_2}{k_{\text{eff}}} \frac{\partial k_{\text{eff}}}{\partial k_2}\bigg|_{k_1} \tag{6}$$

Likewise, by exchanging k_2 for k_1, the sensitivity of k_{eff} to the continuous phase can also be determined. It is easily shown that this sensitivity analysis follows a "sum rule", namely $S_{k_2} + S_{k_2} = 1$.

For the three analytical models described above, expressions for S_{k_2} are derived and given as,

$$S_{k_2,\ \text{Rule of Mixtures}} = \frac{k_2}{k_{\text{eff}}} V_2 \tag{7}$$

$$S_{k_2,\ \text{Maxwell Garnett}} = \frac{k_2 V_2}{k_{\text{eff}}} \left(\frac{3k_1}{k_1(2+V_2) + k_2(1-V_2)} \right)^2 \tag{8}$$

$$S_{k_2,\ \text{Bruggeman}} = \frac{k_2}{k_{\text{eff}}} \left(\frac{k_1 + k_{\text{eff}}(3V_2 - 1)}{4k_{\text{eff}} + k_1(3V_2 - 2) - k_2(3V_2 - 1)} \right) \tag{9}$$

III. Results and Discussion

(1) Microstructure and Phase Characterization

Samples are 98%–99% dense (Table I), with the second phase fairly homogeneously distributed throughout the 8 mol % YSZ microstructure (Fig. 2). The second phase limits the grain growth of 8 mol% YSZ due to grain-boundary pinning and results in a reduction in grain size (Table I). Higher amounts of the second phase are more effective in reducing the grain size. The larger reduction in grain size in the alumina composite compared with the mullite composite (Fig. 2) could be due to differences in either powder particle agglomeration or grain growth and transport rates of the second phase. However, the final grain sizes are much larger than nanoscale dimensions where the high density of grain boundaries would significantly decrease thermal conductivity.[41] XRD of all compositions shows no additional phase formation during sintering (Fig. 3).

(2) Thermal Conductivity Measurements

The 3ω thermal conductivity of most composites decreases slightly as testing temperature is increased (Fig. 4). 20 vol% alumina has the largest thermal conductivity compared with

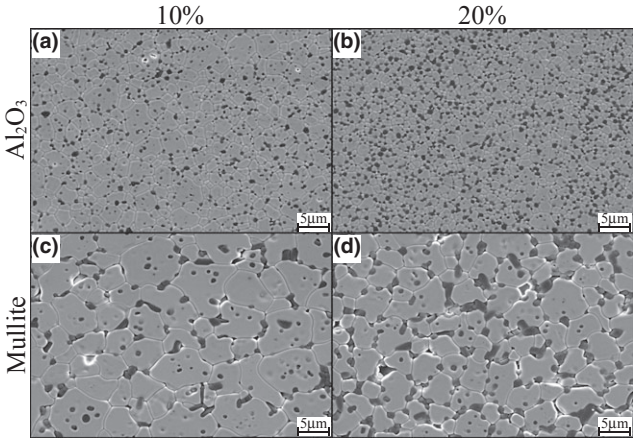

Fig. 2. Scanning electron microscopy micrographs of 8 mol% YSZ (light phase) and dispersed phase (dark phase, alumina, or mullite) for (a) 10 vol% Al_2O_3; (b) 20 vol% Al_2O_3; (c) 10 vol% mullite; and (d) 20 vol% mullite.

Table I. Theoretical Density, Relative Density, and Average Grain Size of 8 mol% YSZ with and Without Second Phase Additions of Alumina and Mullite

	Theoretical density (g/cm^3)	Relative density (%)	8YSZ Grain size (μm)	Al_2O_3 grain size (μm)	Mullite grain size (μm)
8YSZ	6.0	98	9.2 ± 3.5	–	–
8YSZ + 10 vol% Al_2O_3	5.8	99	1.7 ± 0.8	0.9 ± 0.2	–
8YSZ + 20 vol% Al_2O_3	5.6	99	1.2 ± 0.9	0.8 ± 0.1	–
8YSZ + 10 vol% mullite	5.7	98	4.7 ± 1.6	–	1.8 ± 0.3
8YSZ + 20 vol% mullite	5.4	99	3.4 ± 1.2	–	2.0 ± 0.4

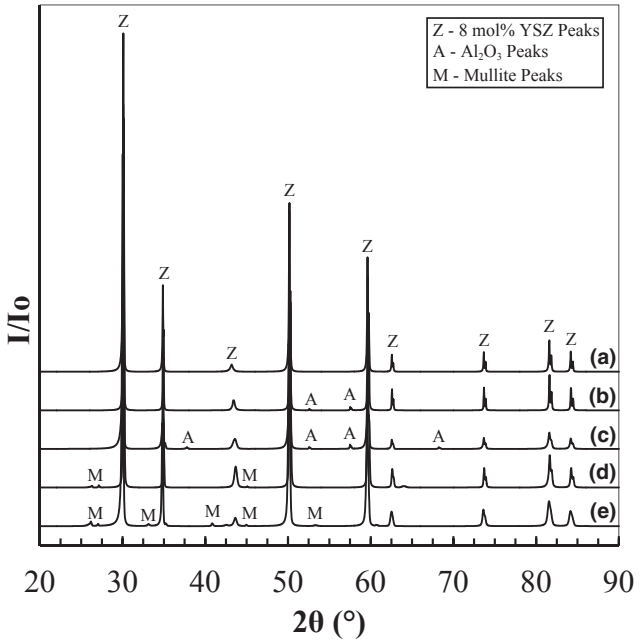

Fig. 3. X-ray diffraction of samples (a) 8 mol% YSZ; (b) +10 vol% Al_2O_3; (c) +20 vol% Al_2O_3; (d) +10 vol% mullite; and (e) +20 vol% mullite.

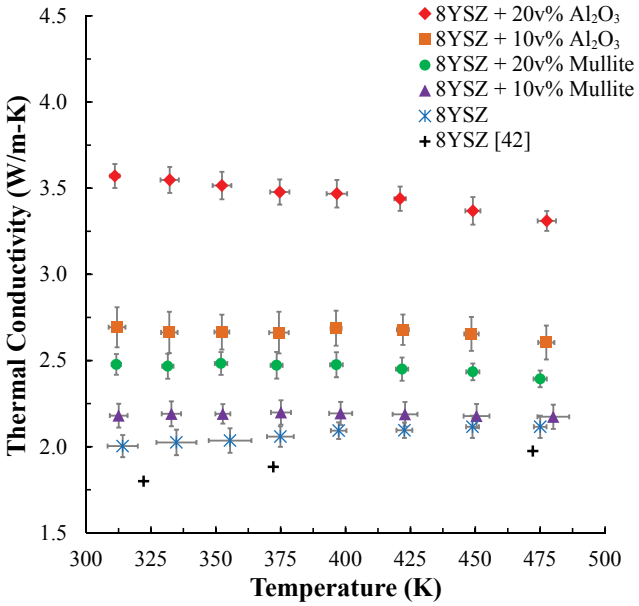

Fig. 4. Measurements of thermal conductivity with experimental uncertainty for single phase 8YSZ and composites using 3ω method. 8YSZ data from[42] included for comparison.

single phase 8 mol% YSZ, followed by 10 vol% alumina, 20 vol% mullite, and 10 vol% mullite, with 10 vol% mullite only slightly higher than single-phase 8 mol% YSZ (Fig. 4). The large increase in thermal conductivity for alumina-containing composites is due to the relatively high thermal conductivity, $k_{\text{alumina, RT}} \approx 33$ W/mK[40] compared to 8 mol % YSZ, $k_{8\text{ mol\% YSZ, RT}} \approx 1.8$–2.4 W/mK,[42–44] while the smaller increase in thermal conductivity in mullite composites can be attributed to mullite having a much lower thermal conductivity than alumina, $k_{\text{mullite, RT}} \approx 6$ W/mK.[38] The thermal conductivity of single phase 8 mol% YSZ increases slightly from room temperature to approximately 400 K (127°C), where it plateaus, and agrees with published data within 8% deviation.[42,43] Interestingly, 10% mullite in 8 mol % YSZ results in almost constant thermal conductivity over

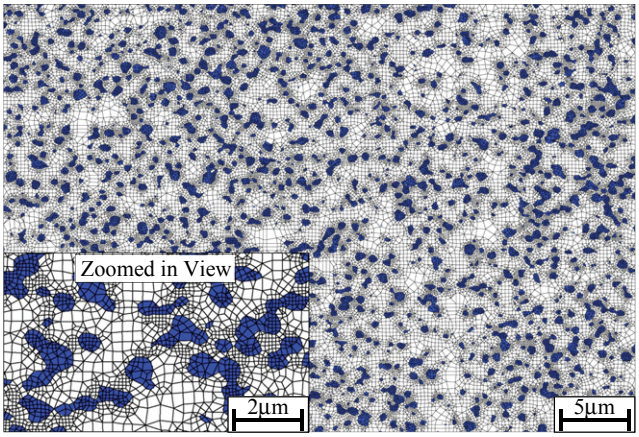

Fig. 5. OOF2 meshing for 8 mol% YSZ (white) + 20 vol% Al_2O_3 (blue if color or dark if B&W). Image correlates to Fig. 2(b). A finer mesh and higher node density along the phase interface can be seen in the zoomed in view.

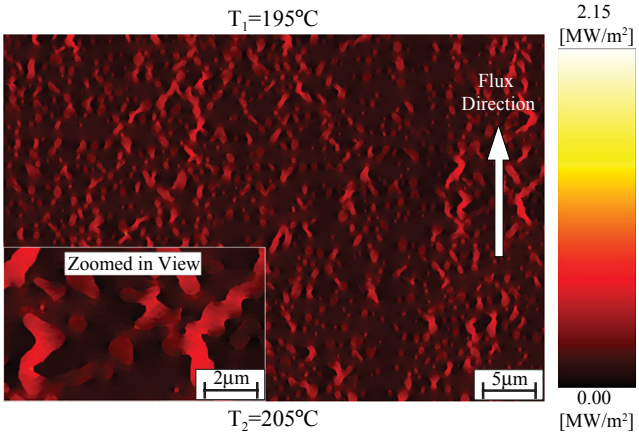

Fig. 6. Heat flux map of 20 vol% alumina corresponding to Fig. 5, produced by OOF2 simulation. Thermal gradient is imposed from bottom to top, keeping sides adiabatic.

the temperature range studied, as the decreasing mullite thermal conductivity effectively counteracts the increasing 8 mol % YSZ conductivity.

A representative OOF2-meshed microstructure of 8 mol% YSZ + 20 vol% alumina is constructed using a combination of triangular and rectangular finite elements, with a larger density of elements located at the interface between two phases (Fig. 5). Further refinement of the mesh did not change the convergence of the solution.

To calculate the effective thermal conductivity for each composite, the heat flux vector is calculated at each node. A heat flux map is generated by taking the scalar magnitude of this vector and illustrates how the second phase creates preferred pathways for heat flow in the direction of the applied temperature gradient, seen in the representative microstructure with an overlaid heat flux map (Fig. 6).

Figures 7 and 8 compare measured thermal conductivity values for 8 mol% YSZ with 10 and 20 vol% second phases with the four theoretical methods (OOF2 simulations, Maxwell Garnett model, Bruggeman model, and linear Rule of Mixtures approximation). The linear Rule of Mixtures exceeded 100% error in some cases, as this approximation overemphasizes the higher thermal conductivity dispersed phase. In these samples, this problem is worst at low temperatures because the contrast between k_1 and k_2 is greatest there (both alumina and mullite have a strongly temperature-dependent conductivity in this regime, scaling approximately as T^{-1}). Figure 9 shows how the linear Rule of Mixtures and

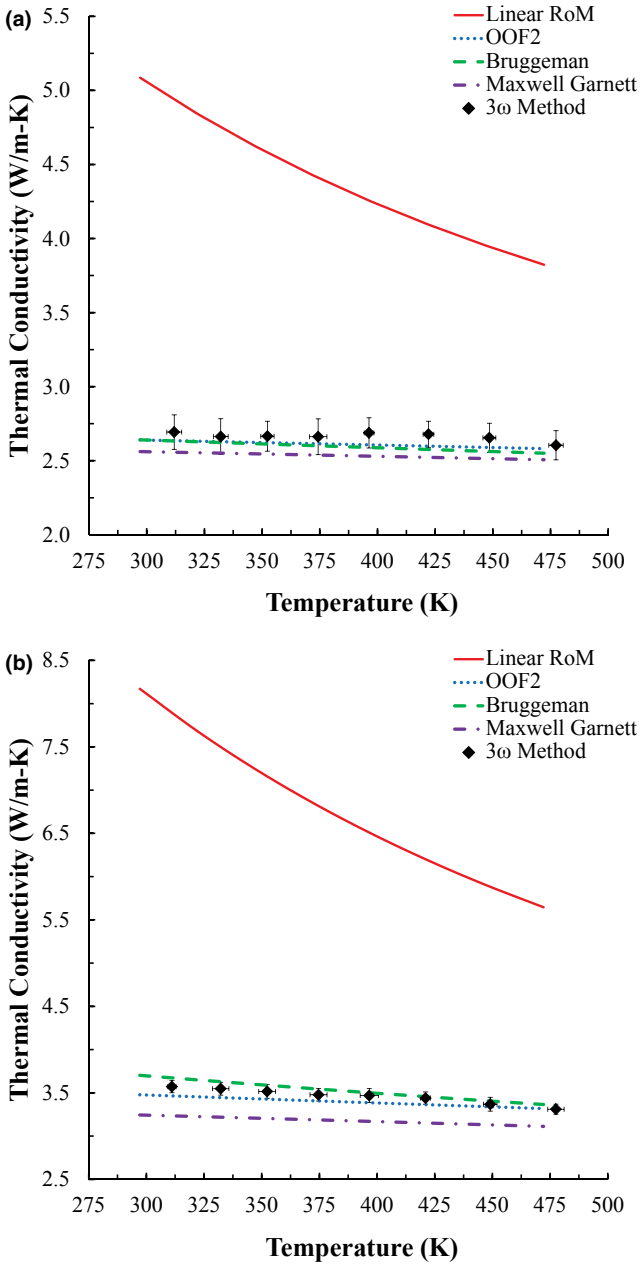

Fig. 7. Comparison of different models with experimental data (3ω method) for thermal conductivity of (a) 8 mol% YSZ + 10 vol% Al_2O_3 and (b) 8 mol% YSZ + 20 vol% Al_2O_3. (Lines: modeled and simulated results. Points: experimental results. Rule of Mixture abbreviated as RoM).

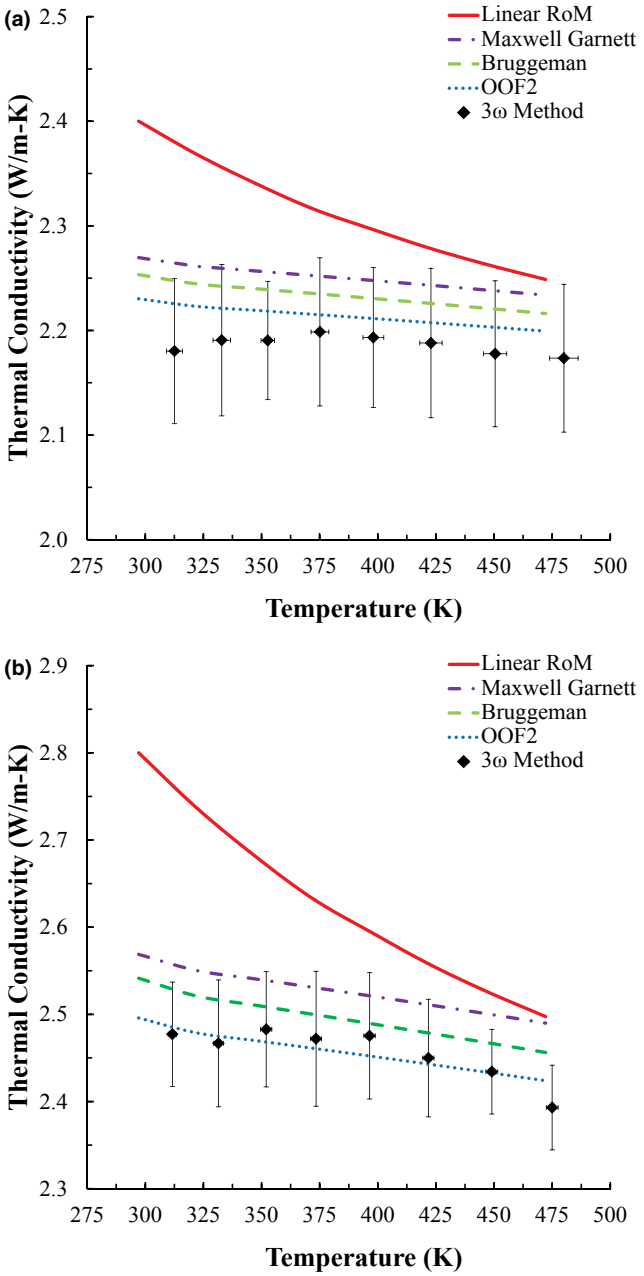

Fig. 8. Comparison of models to 3ω thermal conductivity for (a) 8 mol % YSZ + 10 vol% mullite and (b) 8 mol% YSZ + 20 vol% mullite. (Lines: modeled and simulated results. Points: experimental results.) Thermal conductivity scale expanded compared with Figs. 4 and 7.

the inverse Rule of Mixtures serve as upper and lower bounds for thermal conductivity.

The other three models are within ±8% error or less for each composite. Among these three models, for the 10 and 20 vol% alumina composites the Maxwell Garnett calculations have the worst agreement with the experimental values, ±8% error for 20 vol% alumina and ±5% error for 10 vol% alumina. OOF2 simulations are found to provide only ±2% error compared with experimental values for the 10 vol% alumina composite [Fig 7(a)]. Both OOF2 and Bruggeman produce similar values for the 20 vol% alumina [Fig. 7(b)]; OOF2 gave an underapproximation and Bruggeman an overapproximation, but both models were within ±2% error. As seen in Fig. 8, OOF2 simulations resulted in thermal conductivity values closest to experiments for both 8 mol% YSZ + 10 and 20 vol% mullite composites with only ±1.25% and ±0.5% error, respectively.

Maxwell Garnett and Bruggeman calculations give higher k_{eff} values than OOF2 for mullite composites. The power of the OOF2 simulations is that real microstructures are used, although this is also one of the challenges as SEM images must be obtained, whereas the Maxwell Garnett and Bruggeman models assume simpler distributions and simpler grain shapes. A caveat with OOF2 is that one must ensure that the variability in the real microstructure is accurately represented, hence the use of multiple images from different sections of the material. Also it must be remembered that OOF2 simulations are fundamentally two dimensional, and this may underestimate the true three-dimensional thermal conductivity [see Section III *(3)*]. In this study, allowing for the uncertainty in model inputs (estimated as ±4%), the OOF2 and Bruggeman results both fall within the uncertainty of the experimental results.

(3) 2D Approximations of a 3D Material

It is noteworthy that the OOF2 calculations are so close to the experimental thermal conductivity in Figs. 7 and 8

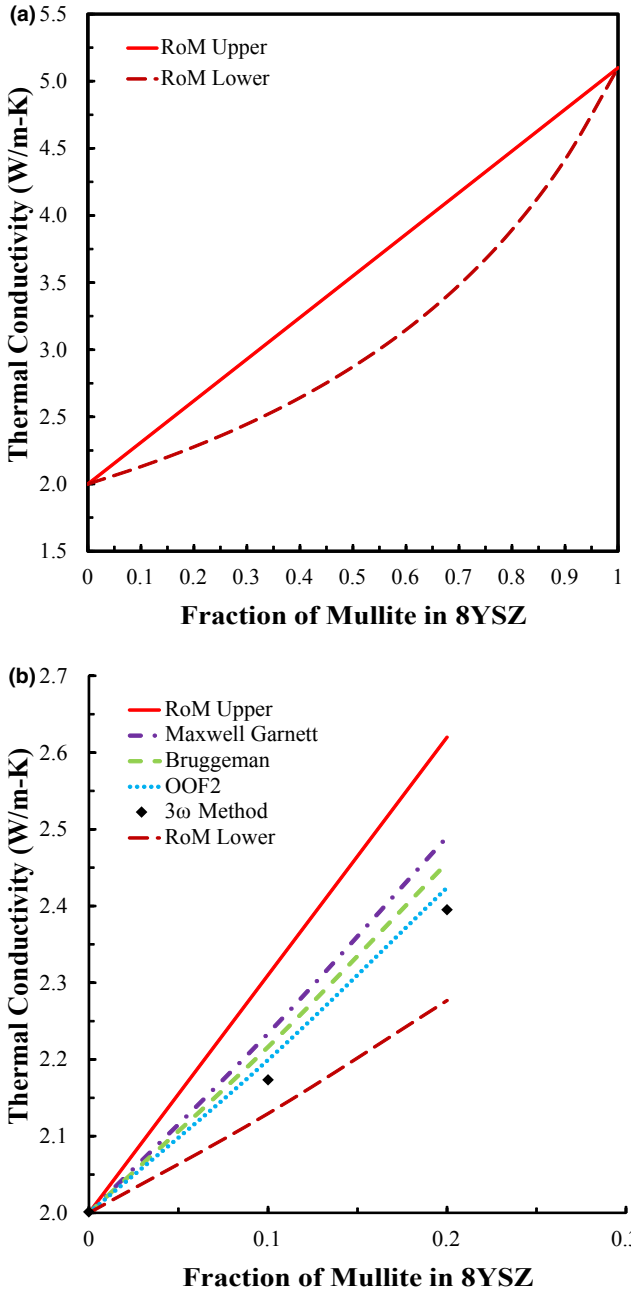

Fig. 9. (a) Linear Rule of Mixtures (upper bound) and inverse Rule of Mixtures (lower bound) for 8YSZ and mullite composites at 200°C; (b) comparison with experimental thermal measurements (3ω method), analytical models, and OOF2.

despite OOF2 being a two-dimensional approach. If the heat flux vectors in a real three-dimensional (3D) system are dominated by flow in a two-dimensional (2D) plane, then an OOF2 analysis of the effective conductivity of this plane will give a very accurate representation of the real 3D conductivity. In terms of Figs. 2, 5, and 6, this would require that all the heat flows in the XY plane, with no local heat fluxes in the Z direction. However, in these samples, the dispersed particles are randomly distributed and approximately equiaxed, and local heat fluxes will have a significantly 3D nature.

To quantify potential errors for approximating a 3D microstructure with a 2D calculation, we can use the known 3D and 2D forms of the Bruggeman model.[45] Recognizing that in the alumina–YSZ composite $k_2/k_1 > 10$, it is a reasonable first approximation and also conservative (worst-case) bound to set $k_2/k_1 \to \infty$, leading to the simplified Bruggeman expressions:

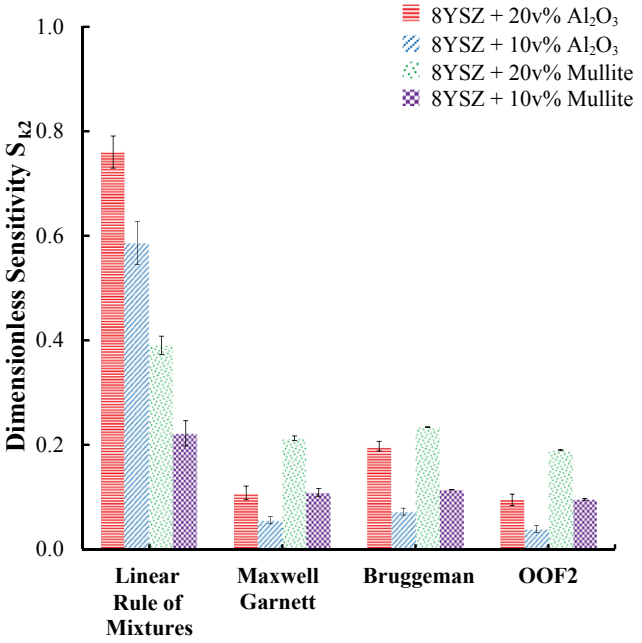

Fig. 10. Average values with standard deviations for the dimensionless sensitivity parameter S_{k_2} for each analytical model and OOF2.

$$3\text{D}: \frac{k_{\text{eff,3D}}}{k_1} = \frac{1}{1-3V_2}, 2\text{D}: \frac{k_{\text{eff,2D}}}{k_1} = \frac{1}{1-2V_2} \tag{10}$$

The 2D expression is traditionally given in terms of an area fraction (e.g., A_2), which here we replace by the volume fraction V_2. This is appropriate because a physically equivalent 3D system can be obtained by extrusion of the same 2D (XY) inclusion geometry uniformly along the third dimension (Z).

The error ratio between the two expressions is:

$$\frac{k_{\text{eff,3D}}}{k_{\text{eff,2D}}} = \frac{1-2V_2}{1-3V_2} \tag{11}$$

Although the specific form of Eq. (11) arose from Bruggeman, the qualitative conclusion that $k_{\text{eff,3D}} > k_{\text{eff,2D}}$ for the same volume fraction can also be reached by comparing 2D and 3D bounding analyses following Elrod.[46] A similar trend is also expected from an argument that reducing the dimensionality is equivalent to imposing additional constraints that also reduce k_{eff}.[45] Thus, regardless of the theory used we conclude that a 2D calculation based on a planar section of a 3D microstructure will underestimate the true 3D conductivity. For the alumina–YSZ composites of the present work, the 3D/2D errors such as estimated from Eq. (11) are likely to be no more than a few tens of percent, with smaller errors as the k_2/k_1 ratio becomes closer to unity (e.g., at higher temperatures and for the mullite–YSZ composites).

(4) Sensitivity

Figure 10 shows the dimensionless sensitivity of k_{eff} to k_2 for each analytical model and OOF2 simulations. The sensitivity parameter S_{k_2} is calculated for each temperature and the average values with standard deviations are reported in Fig. 10. The sensitivity of OOF2 is determined numerically, by increasing the thermal conductivity of the dispersed phase by 5% and calculating the percent increase in k_{eff} relative to the 5% increase.

All four calculations of Fig. 10 exhibit the same trend that S_{k_2} increases with volume fraction V_2 (for fixed k_2). This is

expected because the smaller the V_2, the less the influence k_2 has on k_{eff}. Comparing the alumina and mullite results in Fig. 10, the Maxwell Garnett model, Bruggeman model, and OOF2 simulations also all show that S_{k_2} decreases with increasing k_2 (for fixed V_2). In contrast, the linear Rule of Mixtures model shows an opposite trend of S_{k_2} increasing with k_2, which we now show is nonphysical and thus highlights another shortcoming of the linear Rule of Mixtures approximation.

The physical argument is as follows. As the particles are dispersed and isolated, clearly k_{eff} must saturate to a finite value even in the limit that $k_2 \to \infty$. Therefore, for any fixed V_2, k_{eff} should be most sensitive to k_2 when k_2 and k_1 are of similar magnitudes, while (for a dispersed particle system) S_{k_2} should fall off to zero for both $k_2 \gg k_1$ and $k_2 \ll k_1$. In the present work, k_2 is already larger than k_1, thus explaining why Fig. 10 should show smaller sensitivity to alumina ($k_2/k_1 \approx 16$) than to mullite ($k_2/k_1 \approx 3$). On the other hand, the linear Rule of Mixtures model from Eq. (1) is formally equivalent to conductors in parallel, so in the limit $k_2 \to \infty$ it wrongly gives $k_{\text{eff}} = V_2 k_2$ and $S_{k_2} \to 1$.

To illustrate the impacts of sensitivity on error propagation in the model calculations, we suppose that the uncertainty in the model inputs k_1 and k_2 is around 5%. For the 20 vol% alumina sample, Fig. 9 shows that S_{k_2} for the three preferred models is around 0.15. This means that a 5% uncertainty in k_2 contributes to only around 0.75% uncertainty in k_{eff}. Similarly, using the sum rule stated above we get $S_{k_1} = 0.85$, showing that a 5% uncertainty in k_1 contributes 4.25% uncertainty in k_{eff}. These two error sources are assumed uncorrelated, so their contributions are added in quadrature to obtain a total uncertainty in the calculated k_{eff} of $\sqrt{(0.75\%)^2 + (4.25\%)^2} = 4.3\%$. This is clearly dominated by the uncertainty in the k_1 of the 8 mol% YSZ matrix.

The sensitivity calculations also quantify the potential for further increasing k_{eff} by using inclusions of even higher k_2. For example, at $V_2 = 20$ vol%, replacing alumina by another material with 33% higher thermal conductivity [$k_2 \approx 43$ W/(m·K) rather than 33 (W/(m·K)] would only increase k_{eff} further by around 5%. In the extreme limit $k_2 \to \infty$, for $V_2 = 20\%$ the models show that $k_{\text{eff}}/k_{8\text{ mol\% YSZ}}$ will be at most 2.5 (Bruggeman) or 1.75 (Maxwell Garnett), which shows there still may be some room for improvement compared with the present results ($k_{\text{eff, alumina}}/k_{8\text{ mol\% YSZ}} \approx 1.6$).

(5) Porosity Effects

The effect of porosity on the effective thermal conductivity of bulk ceramics has been considered in a number of previous works,[15,39,42] but not considered in this study, as the samples contained minimal porosity (approximately 1%–2%: Table I). In the limit of small porosity, most standard expressions take the form $k_{\text{eff}} = k_{\text{Fully Dense}} \times (1 - c\phi)$, where ϕ is the porosity and c is a numerical factor. Kingery *et al.*[39] used $c = 1$, Klemens[47] obtained $c = 4/3$, and the Maxwell Garnett [Eq. (3)] and Bruggeman [Eq. (4)] expressions above correspond to $c = 3/2$. Therefore, the present samples with ϕ 2% are expected to have a porosity effect on the thermal conductivity of no more than 3%, which will not significantly impact the results.

IV. Conclusions

Thermal conductivity measurements over a temperature range 310 K (37°C)–475 K (202°C) using the 3ω method show how second phase additions of ceramics with a higher thermal conductivity increase the thermal conductivity of 8YSZ. An 80% increase in thermal conductivity is observed for additions of 20 vol% alumina to 8YSZ in the measured temperature range. Comparison of the Maxwell Garnett, Bruggeman, and linear Rule of Mixtures models with 3ω measurements show the linear Rule of Mixtures is the most divergent from experimentation when predicting thermal conductivity of dilute two-phase composites. Error in the linear Rule of Mixtures model exceeded 100% in some cases, whereas the other two models were within 8% (Maxwell Garnett) and 2.5% (Bruggeman) of measurements. OOF2 simulations provided a good approximation (1.5%) to the measured thermal conductivity. OOF2 has the advantage of incorporating the real microstructure morphology, although OOF2's two-dimensional nature may cause it to underestimate the real three-dimensional thermal conductivity. A dimensionless sensitivity analysis quantified a second shortcoming of the linear Rule of Mixtures, namely that it is far too sensitive to variations in the thermal conductivity of the dispersed phase (k_2). On the other hand, the sensitivity of the three other calculations agree that the overall uncertainty in k_{eff} is determined primarily by the uncertainty in the matrix k_1, especially for the alumina composites with $k_2 \gg k_1$.

Acknowledgment

This research was supported in part by a UC Discovery Grant. Dr. Stephen A. Langer at NIST is thanked for his assistance in using OOF2 simulations.

References

[1]D. R. Clarke, "Interpenetrating Phase Composites," *J. Am. Ceram. Soc.*, **75** [4] 739–59 (1992).
[2]M. C. Martin and M. L. Mecartney, "Grain Boundary Ionic Conductivity of Yttrium Stabilized Zirconia as a Function of Silica Content and Grain Size," *Solid State Ionics*, **161** [1–2] 67–79 (2003).
[3]A. J. Feighery and J. T. S. Irvine, "Effect of Alumina Additions Upon Electrical Properties of 8 mol% Yttria-Stabilised Zirconia," *Solid State Ionics*, **121** [1–4] 209–16 (1999).
[4]M. J. Verkerk, A. J. A. Winnubst, and A. J. Burggraaf, "Effect of Impurities on Sintering and Conductivity of Yttria-Stabilized Zirconia," *J. Mater. Sci.*, **17** [11] 3113–22 (1982).
[5]A. A. E. Hassan, N. H. Menzler, G. Blass, M. E. Ali, H. P. Buchkremer, and D. Stover, "Influence of Alumina Dopant on the Properties of Yttria-Stabilized Zirconia for SOFC Applications," *J. Mater. Sci.*, **37** [16] 3467–75 (2002).
[6]C. K. Yoon and I. W. Chen, "Superplastic Flow of 2-Phase Ceramics Containing Rigid Inclusions-Zirconia Mullite Composites," *J. Am. Ceram. Soc.*, **73** [6] 1555–65 (1990).
[7]D. S. Mclachlan, M. Blaszkiewicz, and R. E. Newnham, "Electrical-Resistivity of Composites," *J. Am. Ceram. Soc.*, **73** [8] 2187–203 (1990).
[8]J. D. Wang and R. Raj, "Activation-Energy for the Sintering of 2-Phase Alumina Zirconia Ceramics," *J. Am. Ceram. Soc.*, **74** [8] 1959–63 (1991).
[9]M. Ishitsuka, T. Sato, T. Endo, and M. Shimada, "Thermal-Shock Fracture-Behavior of ZrO_2 Based Ceramics," *J. Mater. Sci.*, **24** [11] 4057–61 (1989).
[10]M. Mori, T. Abe, H. Itoh, O. Yamamoto, Y. Takeda, and T. Kawahara, "Cubic-Stabilized Zirconia and Alumina Composites as Electrolytes in Planar Type Solid Oxide Fuel-Cells," *Solid State Ionics*, **74** [3–4] 157–64 (1994).
[11]J. Hostasa, W. Pabst, and J. Matejicek, "Thermal Conductivity of Al_2O_3–ZrO_2 Composite Ceramics," *J. Am. Ceram. Soc.*, **94** [12] 4404–9 (2011).
[12]M. R. Winter and D. R. Clarke, "Oxide Materials With low Thermal Conductivity," *J. Am. Ceram. Soc.*, **90** [2] 533–40 (2007).
[13]C. Dames and G. Chen, "1 Omega, 2 Omega, and 3 Omega Methods for Measurements of Thermal Properties," *Rev. Sci. Instrum.*, **76** [1] 2 (2005).
[14]D. G. Cahill, "Thermal Conductivity Measurement from 30 to 750 K: The 3 Omega Method (vol 61, pg 802, 1990)," *Rev. Sci. Instrum.*, **73** [10] 3701–01 (2002).
[15]Z. J. Wang, J. E. Alaniz, W. Y. Jang, J. E. Garay, and C. Dames, "Thermal Conductivity of Nanocrystalline Silicon: Importance of Grain Size and Frequency-Dependent Mean Free Paths," *Nano Lett.*, **11** [6] 2206–13 (2011).
[16]A. C. E. Reid, S. A. Langer, R. C. Lua, V. R. Coffman, S. I. Haan, and R. E. Garcia, "Image-Based Finite Element Mesh Construction for Material Microstructures," *Comput. Mater. Sci.*, **43** [4] 989–99 (2008).
[17]A. C. E. Reid, R. C. Lua, R. E. Garcia, V. R. Coffman, and S. A. Langer, "Modelling Microstructures with OOF2," *Int. J. Mater. Prod. Technol.*, **35** [3–4] 361–73 (2009).
[18]Z. Wang, A. Kulkarni, S. Deshpande, T. Nakamura, and H. Herman, "Effects of Pores and Interfaces on Effective Properties of Plasma Sprayed Zirconia Coatings," *Acta Mater.*, **51** [18] 5319–34 (2003).
[19]K. E. Pappacena, M. T. Johnson, H. Wang, W. D. Porter, and K. T. Faber, "Thermal Properties of Wood-Derived Copper–Silicon Carbide Composites Fabricated via Electrodeposition," *Compos. Sci. Technol.*, **70** [3] 478–84 (2010).
[20]W. D. Kingery, "Thermal Conductivity .14. Conductivity of Multicomponent Systems," *J. Am. Ceram. Soc.*, **42** [12] 617–27 (1959).
[21]R. Landauer, "The Electrical Resistance of Binary Metallic Mixtures," *J. Appl. Phys.*, **23** [7] 779–84 (1952).
[22]A. G. Every, Y. Tzou, D. P. H. Hasselman, and R. Raj, "The Effect of Particle-Size on the Thermal-Conductivity of Zns Diamond Composites," *Acta Metall. Mater.*, **40** [1] 123–9 (1992).

[23]N. J. Kidner, N. H. Perry, T. O. Mason, and E. J. Garboczi, "The Brick Layer Model Revisited: Introducing the Nano-Grain Composite Model," *J. Am. Ceram. Soc.*, **91** [6] 1733–46 (2008).
[24]G. A. Niklasson, C. G. Granqvist, and O. Hunderi, "Effective Medium Models for the Optical-Properties of Inhomogeneous Materials," *Appl. Opt.*, **20** [1] 26–30 (1981).
[25]D. A. G. Bruggeman, "Calculation of Various Physics Constants in Heterogenous Substances I Dielectricity Constants and Conductivity of Mixed Bodies From Isotropic Substances," *Ann. Phys.*, **24** [7] 636–64 (1935).
[26]N. P. Bansal and D. M. Zhu, "Thermal Conductivity of Zirconia–Alumina Composites," *Ceram. Int.*, **31** [7] 911–6 (2005).
[27]A. Bjorneklett, L. Haukeland, J. Wigren, and H. Kristiansen, "Effective-Medium Theory and the Thermal-Conductivity of Plasma-Sprayed Ceramic Coatings," *J. Mater. Sci.*, **29** [15] 4043–50 (1994).
[28]L. C. Davis and B. E. Artz, "Thermal-Conductivity of Metal-Matrix Composites," *J. Appl. Phys.*, **77** [10] 4954–60 (1995).
[29]Z. M. He, C. Stiewe, D. Platzek, G. Karpinski, E. Muller, S. H. Li, M. Toprak, and M. Muhammed, "Effect of Ceramic Dispersion on Thermoelectric Properties of Nano-ZrO_2/$CoSb_3$ Composites," *J. Appl. Phys.*, **101** [4] 043707 (2007).
[30]R. F. Hill and P. H. Supancic, "Thermal Conductivity of Platelet-Filled Polymer Composites," *J. Am. Ceram. Soc.*, **85** [4] 851–7 (2002).
[31]N. Nitani, T. Yamashita, T. Matsuda, S. Kobayashi, and T. Ohmichi, "Thermophysical Properties of Rock-Like Oxide Fuel With Spinel-Yttria Stabilized Zirconia System," *J. Nucl. Mater.*, **274** [12] 15–22 (1999).
[32]J. Y. Oh, Y. H. Koo, B. H. Lee, and Y. W. Tahk, "Evaluation of the Effective Thermal Conductivity of UO_2 Fuel by Combining Potts Model and Finite Difference Method," *J. Nucl. Mater.*, **414** [2] 320–3 (2011).
[33]N. Tessier-Doyen, X. Grenier, M. Huger, D. S. Smith, D. Fournier, and J. P. Roger, "Thermal Conductivity of Alumina Inclusion/Glass Matrix Composite Materials: Local and Macroscopic Scales," *J. Eur. Ceram. Soc.*, **27** [7] 2635–40 (2007).
[34]D. P. H. Hasselman and L. F. Johnson, "Effective Thermal-Conductivity of Composites with Interfacial Thermal Barrier Resistance," *J. Compos. Mater.*, **21** [6] 508–15 (1987).
[35]A. W. Thompson, "Calculation of True Volume Grain Diameter," *Metallography*, **5** [4] 366–369369 (1972).
[36]R. S. Lima and B. R. Marple, "Nanostructured YSZ Thermal Barrier Coatings Engineered to Counteract Sintering Effects," *Mater. Sci. Eng., A*, **485** [1–2] 182–93 (2008).
[37]C. Amaya, J. C. Caicedo, J. M. Yanez-Limon, R. A. Vargas, G. Zambrano, M. E. Gomez, and P. Prieto, "A non-Destructive Method for Determination of Thermal Conductivity of YSZ Coatings Deposited on Si Substrates," *Mater. Chem. Phys.*, **136** [23] 917–24 (2012).
[38]B. Hildmann and H. Schneider, "Thermal Conductivity of 2/1-Mullite Single Crystals," *J. Am. Ceram. Soc.*, **88** [10] 2879–82 (2005).
[39]W. D. Kingery, J. Francl, R. L. Coble, and T. Vasilos, "Thermal Conductivity .10. Data for Several Pure Oxide Materials Corrected to Zero Porosity," *J. Am. Ceram. Soc.*, **37** [2] 107–10 (1954).
[40]R. G. Munro, "Evaluated Material Properties for a Sintered Alpha-Alumina," *J. Am. Ceram. Soc.*, **80** [8] 1919–28 (1997).
[41]P. G. Klemens, and M. Gell, "Thermal Conductivity of Thermal Barrier Coatings," *Mater. Sci. Eng., A*, **245** [2] 143–9 (1998).
[42]K. W. Schlichting, N. P. Padture, and P. G. Klemens, "Thermal Conductivity of Dense and Porous Yttria-Stabilized Zirconia," *J. Mater. Sci.*, **36** [12] 3003–10 (2001).
[43]S. Raghavan, H. Wang, R. B. Dinwiddie, W. D. Porter, and M. J. Mayo, "The Effect of Grain Size, Porosity and Yttria Content on the Thermal Conductivity of Nanocrystalline Zirconia," *Scripta Mater.*, **39** [8] 1119–25 (1998).
[44]D. P. H. Hasselman, L. F. Johnson, L. D. Bentsen, R. Syed, H. L. Lee, and M. V. Swain, "Thermal-Diffusivity and Conductivity of Dense Polycrystalline ZrO_2 Ceramics - A Survey," *Am. Ceram. Soc. Bull.*, **66** [5] 799–806 (1987).
[45]R. Landauer, "Electrical Conductivity in Inhomogeneous Media," *AIP Conf. Proc.*, **1** [40] 2–45 (1978).
[46]H. G. Elrod, "Two Simple Theorems for Establishing Bounds on the Total Heat Flow in Steady-State Heat-Conduction Problems With Convective Boundary Conditions," *Trans. ASME. Ser. C J. Heat Transfer*, **96** [1] 65–7070 (1974).
[47]P. G. Klemens, "Thermal Conductivity of Inhomogeneous Media," *High Temp. - High Pressures*, **23**, 241–8 (1991). □